ACS APPLIED ELECTRONIC MATERIALS

Article

Cite This: ACS Appl. Electron. Mater. XXXX, XXX, XXX−XXX

pubs.acs.org/acsaelm

Enhanced Thermal Stability of Low-*k* Ethyl-Bridged Organosilicas Using Laser Spike Annealing

Zeming Sun, Robert T. Bell, and Michael O. Thompson*

Materials Science and Engineering, Cornell University, Ithaca, New York 14853, United States

ABSTRACT: Incorporating organic bridges within porous organosilica films is a promising route to achieving required mechanical properties of ultralow-*k* dielectric films. To retain these critical organic bridges during thermal processing, submillisecond laser spike annealing (LSA) of sol−gel-derived, low-*k*, ethyl-bridged organosilica films was investigated. Structural and dielectric properties changes, as a function of the peak annealing temperature between 400 and ∼1400 °C, were determined by using a lateral-gradient LSA technique. Under LSA, the ethyl-bridged structures were found to remain stable to the highest LSA peak temperatures; in contrast, nearly 40% of the bridges were lost by 540 °C under hot plate annealing. Refining of Si−O−Si structures, and porosity generation from remnant porogens, was found to begin above ∼700 °C with densification only occurring ∼350 °C higher. This ability of LSA to retain organic bridges within a silica network during thermal processing may ultimately enable development of high-modulus, low-*k* films for advanced microelectronic applications.

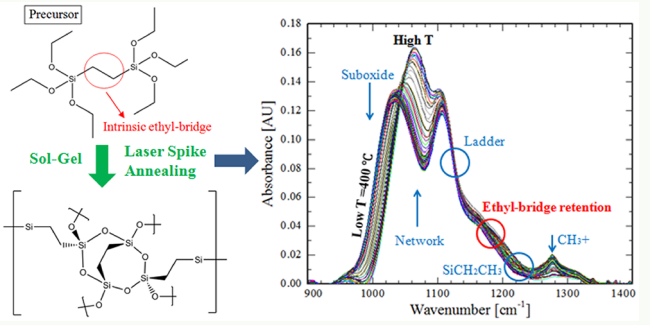

KEYWORDS: *laser spike annealing, carbon-bridged organosilicas, low-k materials, thermal stability, reaction kinetics*

Downloaded by CORNELL UNIV at 09:17:13:965 on June 24, 2019
from https://pubs.acs.org/doi/10.1021/acsaelm.9b00205.

1. INTRODUCTION

Porous low-*k* materials are being developed to overcome limitations induced by interconnection delay in semiconductor devices, with porous silica networks containing organic entities (SiCOH materials) demonstrating dielectric constants (*k*) as low as 2.0.[1−8] While the incorporation of organic groups, together with the presence of pores in the Si−O framework, can dramatically decrease the *k* value, these materials often exhibit poor mechanical strength.[1−7,9−13] To mitigate this problem, alternative processing technologies are required to improve mechanical properties while maintaining dielectric properties. Numerous studies have examined the effects of various annealing techniques, including hot plate/furnace anneal,[14−16] UV radiation,[16−20] electron beam irradiation,[17,21] and plasma treatment.[20,22−24] Volksen first explored the use of laser spike annealing (LSA) to process traditional SiCOH class materials using methyltriethoxysilane as a sol−gel precursor.[25] While Volksen focused on existing low-*k* chemistries, we believe that LSA can be best optimized by considering alternative chemistries that exploit the unique short-time, high-temperature processing environment.

Starting from investigations of bridged periodic mesoporous organosilicas (PMO),[26−31] previous studies identified organic bridges as a potential route to high-performance, low-*k* materials within a sol−gel process.[32−46] Unfortunately, the limited thermal stability of these bridges hinders wider acceptance of sol−gel based PMOs; calcination associated with sol−gel condensation and surfactant removal requires curing temperatures of 300−450 °C,[31,33−35,44−46] or even 550 °C for 7 h.[28] The bridge motif has been reported to break down during curing with reported temperatures ranging from 350 to 700 °C,[18,26,27,31,34] where the variation is likely due to curing time and pretreatment differences. For example, in one study, Asefa et al. observed complete decomposition by 400 °C at a heating rate of 5 °C/min.[26] The competing constraints of sufficient time/temperature for calcination versus the limited thermal stability of the organic bridges may be addressed by the unique thermal environment during LSA. However, to date, LSA annealing of carbon-bridged organosilicas has not been extensively explored, and a fundamental understanding of the reaction kinetics that occurs in these materials is lacking. In this work, we demonstrate the advantages of LSA in these materials by examining the temperature-dependent rates of key chemical structural evolutions using Fourier-transform infrared spectroscopy (FTIR). FTIR provides direct chemical evidence to enable mechanistic understanding of decomposition kinetics over a wide range of temperatures.

The evolution of ethyl-bridged (Si−CH_2−CH_2−Si) films were examined as a function of temperature using the lateral-gradient LSA (lgLSA) technique.[47] A silane precursor, 1,2-bis(triethoxysilyl)ethane (BTESE), containing ethyl-bridged silica motifs was used in this work to yield films with a high density of bridging structures which can enhance the mechanical stability. On the millisecond time scales of LSA, decomposition of these ethyl bridges is kinetically suppressed, especially compared to hour-scale hot plate anneals.

Received: March 30, 2019
Accepted: May 30, 2019
Published: May 30, 2019

© XXXX American Chemical Society

DOI: 10.1021/acsaelm.9b00205
ACS Appl. Electron. Mater. XXXX, XXX, XXX−XXX

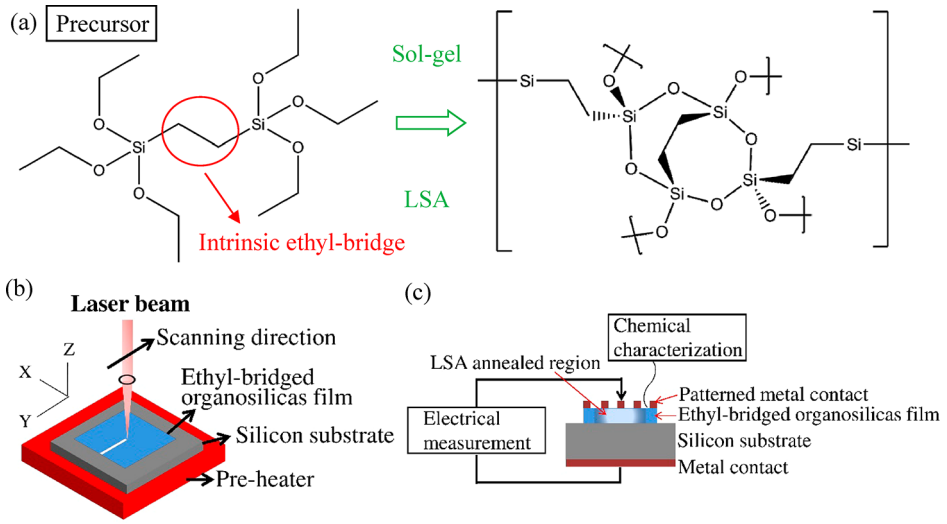

Figure 1. (a) Idealized chemical and network structure of ethyl-bridged organosilica films. (b) Schematic showing laser spike annealing (LSA). (c) Proof-of-concept capacitor device structure for evaluation of spatially resolved chemical and electrical properties.

2. EXPERIMENTAL SECTION

2.1. Sol–Gel Synthesis. Thin films of ethyl-bridged organosilane low-*k* dielectrics on nominally undoped bare Si substrates (native oxide) were prepared by using a sol–gel process.[45,46,48,49] The silane precursor 1,2-bis(triethoxysilyl)ethane (BTESE) and a commercial porogen (Brij-76) were obtained from Sigma-Aldrich. The BTESE and porogen were dissolved separately in 2-methoxy-1-propanol (PMOH) to 25 wt % concentrations. These solutions were then mixed in a porogen/BTESE ratio of 21.5 wt %. To catalyze the sol–gel reaction, 0.61 mL of 1 M nitric acid was added per gram of BTESE. The solution was left standing for 15 min before spin coating directly onto the bare Si wafers at 2000 rpm for 90 s.

Figure 1a shows the idealized chemical and network structure of these ethyl-bridged organosilica films. The ethyl bridges are embedded within the Si–O–Si structures potentially enhancing the network rigidity and hence the mechanical strength. Thermal annealing accelerates the sol–gel process, ultimately resulting in a fully networked Si–O–Si structure. By limiting the time at high temperature using LSA, we can precisely control the degree of the sol–gel transformation.

2.2. Laser Spike Annealing. After spin coating, samples were baked on a hot plate at 85 °C for 2 min, followed by a precure in a vacuum box oven (Yield Engineering Systems, 450PB) at 400 °C for 1 h. This thermal treatment decomposed a substantial fraction of the porogen (as determined by FTIR) leading to an initial porosity. After this initial anneal, films were nominally 300 nm in thickness as measured by a P10 profilometer. For reference to conventional heat treatment, several samples were then subsequently annealed on a hot plate in air for 2 h at temperatures from 400 to 540 °C.

Films were annealed by LSA using a 120 W CO_2 laser (λ = 10.6 μm) with a dwell time of 0.5 ms. As shown in Figure 1b, the CO_2 laser was focused to a line beam with an ~95 μm short axis and an ~700 μm long axis. To induce free carrier absorption in the nominally undoped Si substrate, samples were preheated to a substrate temperature of 400 °C. To follow the structural evolution as a function of temperature, the lateral gradient (single-stripe) LSA (lgLSA) technique was used. In this technique, the incident laser was intentionally focused to a near Gaussian profile orthogonal to the scan direction allowing spatially resolved property measurements to be converted to measurements as a function of the peak annealing temperature.[47]

Peak temperatures during LSA were calibrated as described previously with an estimated uncertainty of 10% (e.g., ±140 °C at 1400 °C).[47,50] These calibrations allowed film property measurements, taken laterally across laser scans, to be linked with specific peak annealing temperatures. Samples were annealed at peak temperatures up to the damage threshold of the silicon substrates near 1400 °C.

2.3. Chemical and Electrical Characterization. Films were characterized using a number of spatially resolved probes, as illustrated in Figure 1c. To determine chemical structure changes, transmission FTIR spectra were collected using a 20 μm diameter aperture in a Bruker Hyperion spectrometer every 25 μm across each scan. Film thicknesses were determined by using a P10 profilometer, with thickness uncertainty mainly determined by the surface morphology.

To measure the dielectric properties, samples were photolithographically patterned, after LSA anneals, to form 20 μm × 12 mm MIS (metal–insulator–semiconductor) capacitors (long axis aligned with the laser scan direction) for *C*–*V* (capacitance-voltage) characterization (Figure 1c). Liftoff lithography, using an ammonia-based image reversal process (90 °C/45 min) to minimize potential damage to the dielectric, was used to pattern 300 nm Al lines deposited by thermal evaporation. These metal capacitor lines included periodic narrowing "cutouts" to permit FTIR measurements across the same samples. *C*–*V* characteristics of the MIS capacitors were measured using an HP 4284A LCR meter at 100 kHz with a 20–35 V dc bias (strong accumulation). Dielectric values were extracted from capacitance and thickness measurements.

3. RESULTS AND DISCUSSION

3.1. Structural Evolution after LSA. Figure 2 shows typical FTIR spectra for a range of LSA peak temperatures, and Table 1 summaries the most prominent peak positions observed and the corresponding chemical bonds. Two general structure sets were analyzed: Si–O bonding structures and organic groups. In Figure 2a, the commonly observed Si–O motifs (including the organic suboxide SiO_xC_y, fully networked Si–O–Si structures, and so-called ladder structures) are detailed.[2,8,14,23,51–53] The two limiting conditions at ~1400 and 400 °C are shown in Figure 2c,d and provide a clear demonstration of the thermally induced changes. Initially films contain almost no fully networked Si–O motifs. As the peak annealing temperature increases, the peak corresponding to suboxides disappears as the fully networked peak develops. To quantitatively follow the structural development, the Si–O and organic molecular peaks were fit using six Gaussian peaks: suboxides at 1035 cm^{-1}, fully networked Si–O–Si structures at 1065 cm^{-1}, ladder structures at 1105 cm^{-1}, the Si–CH_2–CH_2–Si bridge at 1162 cm^{-1}, the Si–CH_2CH_3 peak at 1220

DOI: 10.1021/acsaelm.9b00205
ACS Appl. Electron. Mater. XXXX, XXX, XXX–XXX

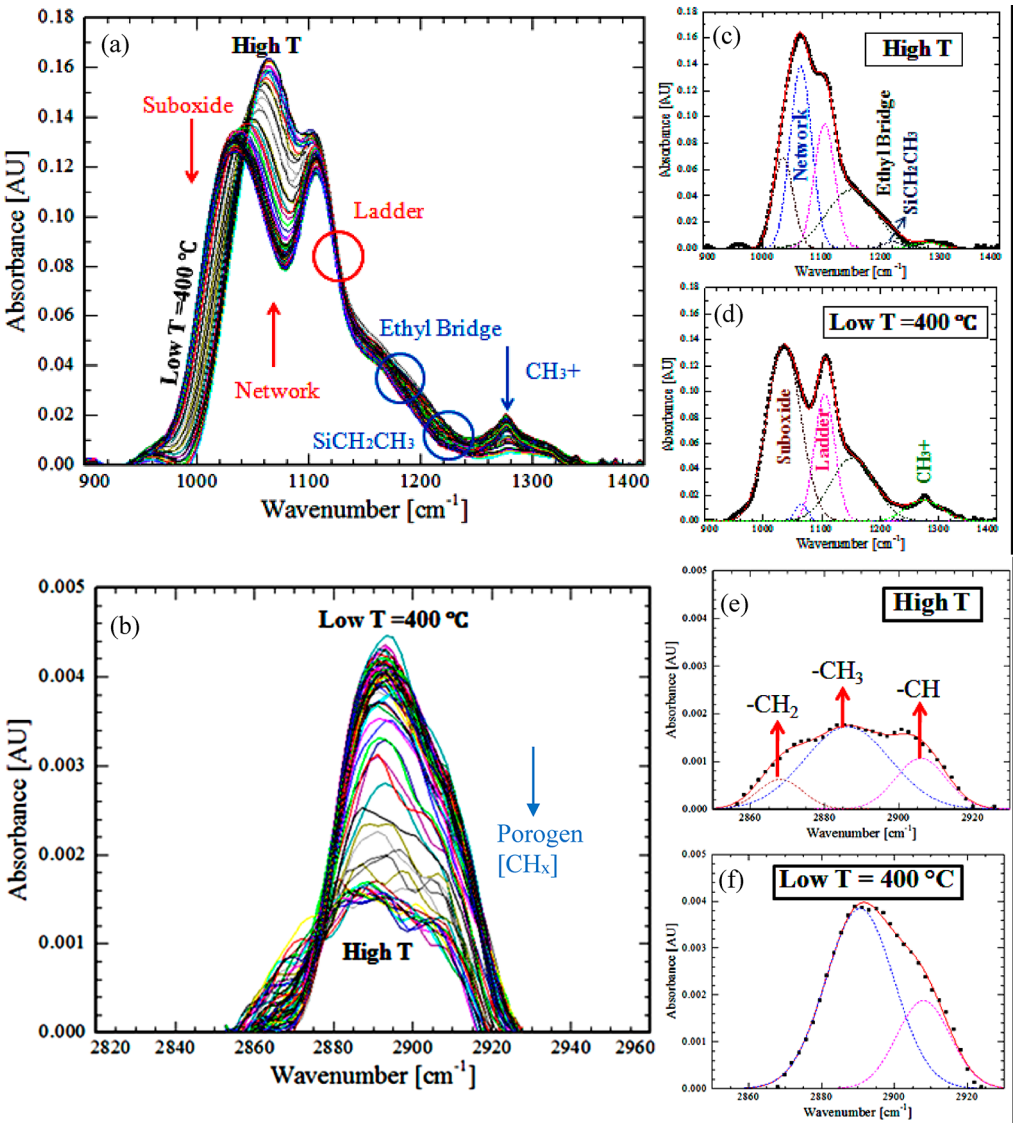

Figure 2. FTIR spectra for a range of LSA peak temperatures from 400 to near 1400 °C. (a) Wavelength range containing Si−O motifs with arrows or circles marking the positions and evolution trends of various structures. (b) Wavelength range corresponding to porogen structures. Individual spectra at the limiting temperatures of ∼1400 °C (c, e) and 400 °C (d, f).

Table 1. Summary of FTIR Peak Positions Associated with Interpreted Bonds

	Si−O−Si structures					
bonds	suboxide	fully networked Si−O−Si				ladder
peak position (cm^{-1})	1035	1065				1105
	organic structures					
	ethyl chain	ethyl bridge		CH_x (porogen)		
bonds	Si−CH_2CH_3	Si−CH_2−CH_2−Si	CH_3+	−CH	−CH_2	−CH_3
peak position (cm^{-1})	945−975 and 1220	1162	1275	2906	2865	2887

cm^{-1}, and a complex CH_3+ methyl peak at 1275 cm^{-1}.[2,8,14,23,51−53] (The peak at 1275 cm^{-1} includes both the CH_3 methyl bending mode convoluted with additional CH_x modes; these were fit as a single peak and are designated CH_3+ in the following discussion.) All fits exhibited very low and uniform residuals (as a function of annealing temperature), indicating that all major peaks were likely included in this modeling.

Figure 2b shows the evolution of CH_x peaks with increasing LSA temperature. These CH_x peaks (2850−2930 cm^{-1}) and the CH_3+ peak (1240−1320 cm^{-1}) in Figure 2a arise primarily from the porogen. Within the 2850−2930 cm^{-1} CH_x band, there are three overlapping subpeaks: −CH at 2906 cm^{-1}, −CH_2 at 2865 cm^{-1}, and −CH_3 at 2887 cm^{-1}.[8,53] As shown in Figure 2c−f, the −CH_3, −CH, and CH_3+ peaks all diminish with temperature; in contrast, the new −CH_2 peak appears at high temperature. In subsequent discussion, the −CH, −CH_2, and −CH_3 peaks will be denoted collectively as a single CH_x porogen peak.

The areas of the absorbance peaks for these motifs, as a function of the peak annealing temperature, are summarized in Figure 3. Below 700 °C (for the 0.5 ms dwell), no structural changes are observed. As the anneal temperature increases above 700 °C, the suboxide motif begins to disappear and is replaced with the fully networked structure (Figure 3a). In contrast, the ladder motif remains essentially unchanged to the

DOI: 10.1021/acsaelm.9b00205
ACS Appl. Electron. Mater. XXXX, XXX, XXX−XXX

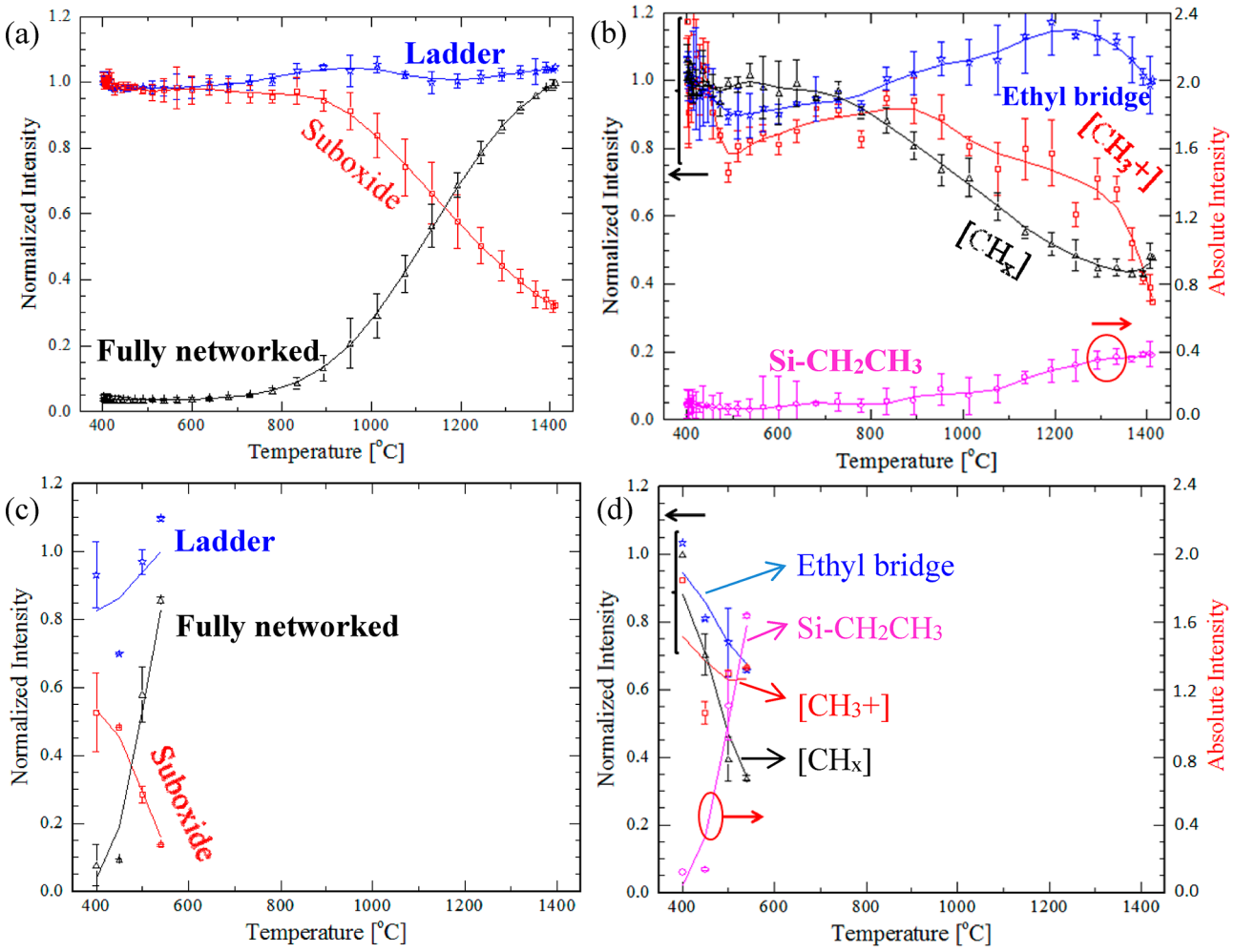

Figure 3. Temperature-dependent structural evolution by LSA (a, b) and hot plate (c, d) annealing. The fully networked peaks are normalized to the high-temperature LSA limit, the Si−CH_2CH_3 peak (1220−1250 cm^{-1}) values are absolute absorbance, and all other peaks are normalized to the unannealed values. (a) Si−O−Si and (b) organic structure peak intensities as a function of the peak LSA temperature. (c) Si−O−Si and (d) organic structure peak intensities after 2 h hot plate anneals.

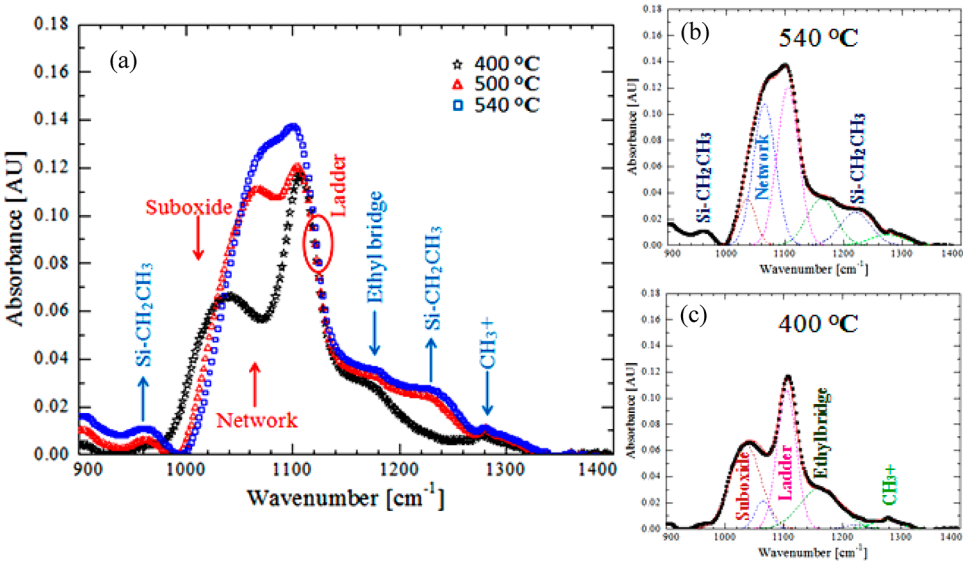

Figure 4. FTIR spectra for hot plate annealed samples at temperatures from 400 to 540 °C. (a) The region containing Si−O motifs is shown with arrows or circles marking the positions and evolution trends of various structures. (b, c) Specific peak fitting at 540 and 400 °C.

DOI: 10.1021/acsaelm.9b00205
ACS Appl. Electron. Mater. XXXX, XXX, XXX−XXX

highest temperatures explored. Although the onset of the network formation and suboxide loss are difficult to establish precisely, these data suggest that some limited network formation does occur prior to loss of the suboxide peak, indicating structural relaxation of other unstable entities. At the highest temperatures, the network peak increases in intensity by nearly a factor of 26, while the suboxide peak intensity decreases by a factor of 3.

The $Si-CH_2-CH_2-Si$ (ethyl) bridges (Figure 3b) that remain after the initial oven anneal are surprisingly stable and remain intact to the highest LSA temperatures explored. The observed ~10% variation in the intensity of this peak is likely an artifact of fitting (Figure 2a) this highly convoluted peak; no loss of these bridges appears to occur for any temperature on this time scale. The $Si-CH_2CH_3$ structure that would most likely form from thermal decomposition of the ethyl bridges correspondingly remains extremely low below 1100 °C with only a slight increase at higher temperatures. Indeed, compared to hot plate anneals to 540 °C (Figure 3d), the $Si-CH_2CH_3$ for the highest temperature LSA anneal is only 25% as intense and further confirms retention of the ethyl bridges. The enhanced thermal stability of these ethyl bridges is significant and should allow retention of mechanical properties during pore creation.

In contrast, the CH_3+ peak (1240−1320 cm^{-1}) and the CH_x peaks (2850−2930 cm^{-1}), both arising from the porogen, decrease continuously with increasing temperature. These peaks correspond to further disassociation of remnant porogen and nanoscale pore formation. Above 700 °C, porogen loss during LSA becomes observable. This behavior confirms that LSA can effectively decompose organic groups, resulting in a high porosity. At the highest LSA temperatures, the CH_3+ peak continues to decrease, which is consistent with film densification (see text below). However, the CH_x peak appears to saturate at a nonzero value which is likely due to signal from stable ethyl bridges.

3.2. Comparison with Hot Plate Annealing. Figure 4 shows comparable data for the structural evolution as a function of hot plate annealing temperatures. Several distinctive behaviors, relative to LSA, are observed. As shown quantitatively in Figure 3c, hot plate annealing results in similar loss of suboxide motifs and development of fully networked motifs with increasing temperature. However, while the ladder motif remains relatively stable under both hot plate and LSA annealing, the suboxide motif is rapidly lost for hot plate anneals with <10% remaining after a 540 °C anneal. In contrast, under LSA, over 30% of this suboxide peak intensity persists at high temperature, indicating retention of ethyl bridges. This suggests that complex bridging organic structures are unstable on hot plate time scales, but their decomposition is kinetically suppressed on submillisecond time scales.

Changes in the organic structural peaks (Figure 3d) are consistent with this interpretation also. The CH_3+ and CH_x peaks decrease as the porogen decomposes with temperature. But the ethyl bridge peak intensity also decreases by 40% at 540 °C compared to essentially no change during LSA. With the loss of the ethyl bridges, the $Si-CH_2CH_3$ structure peak at 1220 cm^{-1} rapidly increases to a value of 1.6 (compared to only 0.4 for LSA at the highest temperature). Because of the increased loss of the ethyl bridges, a new peak at 945−975 cm^{-1}, also corresponding to the $Si-CH_2CH_3$ structure, is observed (Figure 4b).[52] These results again confirm the instability of the complex bridging structure on hot plate time scales.

The retention of the ethyl bridges under LSA is critical to improving mechanical properties while also maintaining a low k value. Annealing on millisecond time scales to temperatures above 1000 °C is likely to be effective for processing these types of low-k dielectrics.

3.3. MIS Electrical Properties after LSA. Figure 5 shows the film thickness and dielectric constant evolution as a function of temperature, as determined from direct measurements on metal−insulator−semiconductor (MIS) structures. Below 1100 °C, no densification (thickness changes) is observed. As temperatures increase above 1100 °C, films begin to densify, indicating aggregation of nanocrystals and collapse of nanopores.[54] At the highest temperature, the film thickness decreases by 20% from the unannealed value. This densification, while improving the mechanical properties including modulus, will almost certainly result in a detrimental increase in the effective k value. Indeed, measurements of the modulus by nanoindentation mirrored this densification, remaining essentially constant below 1100 °C before increasing by 20% at the highest temperatures.

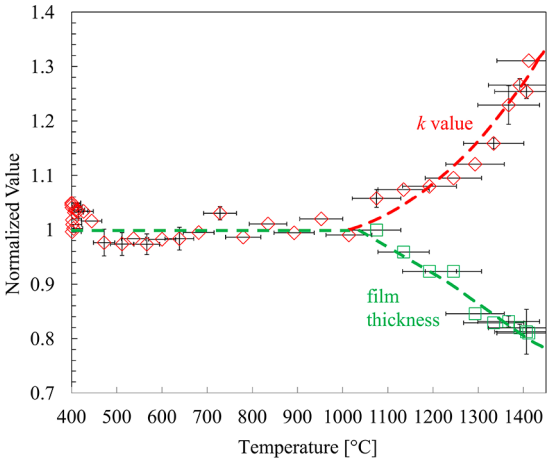

Figure 5. Normalized film thickness (densification) and dielectric constant as a function of the peak LSA annealing temperature. Dashed lines are meant as guides to the eye only.

Initial k values, after the 400 °C 1 h vacuum precure that would have activated a large fraction of the porogen, were ~2.5; this is slightly higher than the 2.3 value reported for a similar material.[45] For anneals <1000 °C, the dielectric constant remains essentially unchanged (within measurement variability). However, with higher temperatures the dielectric constant begins to increase, ultimately reaching a value 30% higher.

3.4. Summary of Threshold Temperatures after LSA. The results of this study are summarized in Table 2. Two important threshold temperatures for the 0.5 ms LSA anneal are identified. At 700−800 °C, structural transformation from the suboxide to a fully networked Si−O−Si structure occurs; in this range, the dielectric constant remains essentially unchanged. This behavior indicates that additional porogen decomposition and pore generation in this temperature range are offset by the increased network formation. At higher temperatures, near 1000−1100 °C, the increased network connectivity leads to densification impacting the dielectric constant and likely the modulus. These findings suggest that

DOI: 10.1021/acsaelm.9b00205
ACS Appl. Electron. Mater. XXXX, XXX, XXX−XXX

Table 2. Summary of Threshold Temperatures for LSA Effects

effects	temp (°C)	effects	temp (°C)
loss of ethyl bridges	>1400	onset of densification	~1100
initial removal of porogen	~700	onset of *k* value increase	~1000
conversion to fully networked bonding	~700	completion of porogen removal	~1200

LSA may provide an effective path to annealing these materials, providing retention of ethyl bridges in the organic/inorganic mesoporous structures while also fully relaxing the inorganic phase, decomposing porogens, and retaining critical porosity.[55−57]

4. CONCLUSIONS

In conclusion, low-*k* dielectric films with ethyl bridges were successfully synthesized using a sol−gel process followed by an LSA anneal. Structural and dielectric properties as a function of peak annealing temperature were determined using the lateral-gradient LSA technique. Ethyl bridge structures within the silica network remain stable under submillisecond annealing to temperatures above 1400 °C while they are lost by 540 °C under hour duration hot plate anneals. Porogen decomposition similarly begins above 700 °C, at the same temperature as Si−O−Si motifs are refined. Densification of the film, and the corresponding increase in dielectric constant, is only observed as anneal temperatures increase above 1000−1100 °C. This thermal stability of ethyl bridges during millisecond LSA should enable much wider application of carbon-bridged PMO materials in general.

AUTHOR INFORMATION

Corresponding Author

*E-mail: mot1@cornell.edu (M.O.T.).

ORCID

Zeming Sun: 0000-0001-5816-5578

Robert T. Bell: 0000-0003-0923-6012

Notes

The authors declare no competing financial interest.

ACKNOWLEDGMENTS

The work was supported by the Semiconductor Research Corporation (SRC, Task ID 2071.018 "Laser Annealing of Porous SiOCH-Class Low-K Dielectrics for Optimized Mechanical Properties"), GlobalFoundries, and Intel. The authors thank the Cornell Nanoscale Science and Technology Facility (CNF), a member of the National Nanotechnology Coordinated Infrastructure, which is supported by the National Science Foundation (NSF, Grant ECCS-1542081), and the Cornell Center for Materials Research (CCMR), which is supported through the NSF MRSEC program (DMR-1719875) for use of their facilities. Z.S. acknowledges Yao Sun, Duhan Zhang, and Prof. Wiesner for experimental assistance.

REFERENCES

(1) Volksen, W.; Miller, R. D.; Dubois, G. Low Dielectric Constant Materials. *Chem. Rev.* **2010**, *110*, 56−100.

(2) Grill, A.; Gates, S. M.; Ryan, T. E.; Nguyen, S. V.; Priyadarshini, D. Progress in the Development and Understanding of Advanced Low *k* and Ultralow *k* Dielectrics for Very Large-Scale Integrated Interconnects-State of the Art. *Appl. Phys. Rev.* **2014**, *1*, 011306.

(3) Shamiryan, D.; Abell, T.; Iacopi, F.; Maex, K. Low-*k* Dielectric Materials. *Mater. Today* **2004**, *7*, 34−39.

(4) Hatton, B. D.; Landskron, K.; Hunks, W. J.; Bennett, M. R.; Shukaris, D.; Perovic, D. D.; Ozin, G. A. Materials Chemistry for Low-*k* Materials. *Mater. Today* **2006**, *9*, 22−31.

(5) Nguyen, C. V.; Carter, K. R.; Hawker, C. J.; Hedrick, J. L.; Jaffe, R. L.; Miller, R. D.; Remenar, J. F.; Rhee, H. W.; Rice, P. M.; Toney, M. F.; Trollsas, M.; Yoon, D. Y. Low-Dielectric, Nanoporous Organosilicate Films Prepared via Inorganic/Organic Polymer Hybrid Templates. *Chem. Mater.* **1999**, *11*, 3080−3085.

(6) Morgen, M.; Ryan, E. T.; Zhao, J. H.; Hu, C.; Cho, T.; Ho, P. S. Low Dielectric Constant Materials for ULSI Interconnects. *Annu. Rev. Mater. Sci.* **2000**, *30*, 645−680.

(7) Maex, K.; Baklanov, M. R.; Shamiryan, D.; Lacopi, F.; Brongersma, S. H.; Yanovitskaya, Z. S. Low Dielectric Constant Materials for Microelectronics. *J. Appl. Phys.* **2003**, *93*, 8793−8841.

(8) Grill, A.; Neumayer, D. A. Structure of Low Dielectric Constant to Extreme Low Dielectric Constant SiCOH Films: Fourier Transform Infrared Spectroscopy Characterization. *J. Appl. Phys.* **2003**, *94*, 6697−6707.

(9) Si, L.; Guo, D.; Xie, G.; Luo, J. Mechanical Properties and Interface Characteristics of Nanoporous Low-*k* Materials. *ACS Appl. Mater. Interfaces* **2014**, *6*, 13850−13858.

(10) Stan, G.; Gates, R. S.; Kavuri, P.; Torres, J.; Michalak, D.; Ege, C.; Bielefeld, J.; King, S. W. Mechanical Property Changes in Porous Low-*k* Dielectric Thin Films during Processing. *Appl. Phys. Lett.* **2014**, *105*, 152906.

(11) Volinsky, A. A.; Vella, J. B.; Gerberich, W. W. Fracture Toughness, Adhesion and Mechanical Properties of Low-*k* Dielectric Thin Films Measured by Nanoindentation. *Thin Solid Films* **2003**, *429*, 201−210.

(12) Wang, Y. H.; Moitreyee, M. R.; Kumar, R.; Wu, S. Y.; Xie, J. L.; Yew, P.; Subramanian, B.; Shen, L.; Zeng, K. Y. The Mechanical Properties of Ultra-Low-Dielectric-Constant Films. *Thin Solid Films* **2004**, *462−463*, 227−230.

(13) Raymunt, A. M.; Bell, R. T.; Thompson, M. O.; Clancy, P. Effect of Laser Annealing on the Structure of Amorphous Porous SiCOH Materials. *J. Phys. Chem. C* **2015**, *119*, 12616−12624.

(14) Das, G.; Mariotto, G.; Quaranta, A. Microstructural Evolution of Thermally Treated Low-Dielectric Constant SiOC:H Films Prepared by PECVD. *J. Electrochem. Soc.* **2006**, *153*, F46−F51.

(15) Park, J. M.; Choi, J. K.; An, C. J.; Jin, M. L.; Kang, S.; Yun, J.; Kong, B. S.; Jung, H. T. Nanoporous SiCOH/C_xH_y Dual Phase Films with an Ultralow Dielectric Constant and a High Young's Modulus. *J. Mater. Chem. C* **2013**, *1*, 3414−3420.

(16) Volksen, W.; Magbitang, T. P.; Miller, R. D.; Purushothaman, S.; Cohen, S. A.; Nakagawa, H.; Nobe, Y.; Kokubo, T.; Dubois, G. J. M. A Manufacturing Grade, Porous Oxycarbosilane Spin-On Dielectric Candidate with $k \leq 2.0$. *J. Electrochem. Soc.* **2011**, *158*, G155−G161.

(17) Jousseaume, V.; Zenasni, A.; Favennec, L.; Gerbaud, G.; Bardet, M.; Simon, J. P.; Humbert, A. Comparison Between E-beam and Ultraviolet Curing to Perform Porous a-SiOC:H. *J. Electrochem. Soc.* **2007**, *154*, G103−G109.

(18) Rakhimova, T. V.; Rakhimov, A. T.; Mankelevich, Y. A.; Lopaev, D. V.; Kovalev, A. S.; Vasil'eva, A. N.; Zyryanov, S. M.; Kurchikov, K.; Proshina, O. V.; Voloshin, D. G.; Novikova, N. N.; Krishtab, M. B.; Baklanov, M. R. Low-*k* Films Modification Under EUV and VUV Radiation. *J. Phys. D: Appl. Phys.* **2014**, *47*, 025102.

(19) Sinha, H.; Ren, H.; Nichols, M. T.; Lauer, J. L.; Tomoyasu, M.; Russell, N. M.; Jiang, G.; Antonelli, G. A.; Fuller, N. C.; Engelmann, S. U.; Lin, Q.; Ryan, V.; Nishi, Y.; Shohet, J. L. The Effects of Vacuum Ultraviolet Radiation on Low-*k* Dielectric Films. *J. Appl. Phys.* **2012**, *112*, 111101.

(20) Urbanowicz, A. M.; Vanstreels, K.; Verdonck, P.; Shamiryan, D.; De Gendt, S.; Baklanov, M. R. Improving Mechanical Robustness of Ultralow-*k* SiOCH Plasma Enhanced Chemical Vapor Deposition

DOI: 10.1021/acsaelm.9b00205
ACS Appl. Electron. Mater. XXXX, XXX, XXX−XXX

Glasses by Controlled Porogen Decomposition prior to UV-Hardening. *J. Appl. Phys.* **2010**, *107*, 104122.
(21) Chang, T. C.; Tsai, T. M.; Liu, P. T.; Chen, C. W.; Tseng, T. Y. Study on the Effect of Electron Beam Curing on Low-*k* Porous Organosilicate Glass (OSG) Material. *Thin Solid Films* **2004**, *469*−*470*, 383−387.
(22) Sun, Y.; Krishtab, M.; Struyf, H.; Verdonck, P.; De Feyter, S.; Baklanov, M. R.; Armini, S. Impact of Plasma Pretreatment and Pore Size on the Sealing of Ultra-Low-*k* Dielectrics by Self-Assembled Monolayers. *Langmuir* **2014**, *30*, 3832−3844.
(23) Baklanov, M. R.; De Marneffe, J.; Shamiryan, D.; Urbanowicz, A. M.; Shi, H.; Rakhimova, T. V.; Huang, H.; Ho, P. S. Plasma Processing of Low-*k* Dielectrics. *J. Appl. Phys.* **2013**, *113*, 041101.
(24) Urbanowicz, A. M.; Vanstreels, K.; Shamiryan, D.; De Gendt, S.; Baklanov, M. R. Effect of Porogen Residue on Chemical, Optical, and Mechanical Properties of CVD SiCOH Low-*k* Materials. *Electrochem. Solid-State Lett.* **2009**, *12*, H292−H295.
(25) Volksen, W.; Dubois, G.; Kellock, A.; Magbitang, T. P.; Miller, R. D.; Miller, D.; Cohen, S.; Simonyi, E. E.; Ramirez, L.; Markle, D.; Chen, S.; Zhou, S.; Wang, X.; Wang, Y. Mechanical Enhancement of Low-*k* Organosilicates by Laser Spike Annealing. *J. Electrochem. Soc.* **2008**, *155*, G224−G230.
(26) Asefa, T.; Maclachlan, M. J.; Coombs, N.; Ozin, G. A. Periodic Mesoporous Organosilicas with Organic Groups Inside the Channel Walls. *Nature* **1999**, *402*, 867−871.
(27) Inagaki, S.; Guan, S.; Fukushima, Y.; Ohsuna, T.; Terasaki, O. Novel Mesoporous Materials with a Uniform Distribution of Organic Groups and Inorganic Oxide in Their Frameworks. *J. Am. Chem. Soc.* **1999**, *121*, 9611−9614.
(28) Melde, B. J.; Holland, B. T.; Blanford, C. F.; Stein, A. Mesoporous Sieves with Unified Hybrid Inorganic/Organic Frameworks. *Chem. Mater.* **1999**, *11*, 3302−3308.
(29) Vercaemst, C.; Ide, M.; Wiper, P. V.; Jones, J. T. A.; Khimyak, Y. Z.; Verpoort, F.; Van Der Voort, P. Ethenylene-Bridged Periodic Mesoporous Organosilicas: From E to Z. *Chem. Mater.* **2009**, *21*, 5792−5800.
(30) Goethals, F.; Vercaemst, C.; Cloet, V.; Hoste, S.; Van Der Voort, P.; Van Driessche, I. Comparative Study of Ethylene- and Ethenylene-Bridged Periodic Mesoporous Organosilicas. *Microporous Mesoporous Mater.* **2010**, *131*, 68−74.
(31) Xu, R.; Ibrahim, S. M.; Kanezashi, M.; Yoshioka, T.; Ito, K.; Ohshita, J.; Tsuru, T. New Insights into the Microstructure-Separation Properties of Organosilica Membranes with Ethane, Ethylene, Acetylene Bridges. *ACS Appl. Mater. Interfaces* **2014**, *6*, 9357−9364.
(32) Landskron, K.; Hatton, B. D.; Perovic, D. D.; Ozin, G. A. Periodic Mesoporous Organosilicas Containing Interconnected $[Si(CH_2)]_3$ Rings. *Science* **2003**, *302*, 266−269.
(33) Hatton, B. D.; Landskron, K.; Whitnall, W.; Perovic, D. D.; Ozin, G. A. Spin-Coated Periodic Mesoporous Organosilica Thin Films - Towards a New Generation of Low-Dielectric-Constant Materials. *Adv. Funct. Mater.* **2005**, *15*, 823−829.
(34) Seino, M.; Wang, W.; Lofgreen, J. E.; Puzzo, D. P.; Manabe, T.; Ozin, G. A. Low-*k* Periodic Mesoporous Organosilica with Air Walls: POSS-PMO. *J. Am. Chem. Soc.* **2011**, *133*, 18082−18085.
(35) De Theije, F. K.; Balkenende, A. R.; Verheijen, M. A.; Baklanov, M. R.; Mogilnikov, K. P.; Furukawa, Y. Structural Characterization of Mesoporous Organosilica Films for Ultralow-*k* Dielectrics. *J. Phys. Chem. B* **2003**, *107*, 4280−4289.
(36) Lu, Y.; Fan, H.; Doke, N.; Loy, D. A.; Assink, R. A.; LaVan, D. A.; Brinker, C. J. Evaporation-Induced Self-Assembly of Hybrid Bridged Silsesquioxane Film and Particulate Mesophases with Integral Organic Functionality. *J. Am. Chem. Soc.* **2000**, *122*, 5258−5261.
(37) Hoffmann, F.; Cornelius, M.; Morell, J.; Froba, M. Silica-Based Mesoporous Organic−Inorganic Hybrid. *Angew. Chem., Int. Ed.* **2006**, *45*, 3216−3251.
(38) Van Der Voort, P.; Vercaemst, C.; Schaubroeck, D.; Verpoort, F. Ordered Mesoporous Materials At the Beginning of the Third Millennium: New Strategies to Create Hybrid and Non-Siliceous Variants. *Phys. Chem. Chem. Phys.* **2008**, *10*, 347−360.
(39) Wang, W.; Lofgreen, J. E.; Ozin, G. A. Why PMO? Towards Functionality and Utility of Periodic Mesoporous Organosilicas. *Small* **2010**, *6*, 2634−2642.
(40) Innocenzi, P.; Malfatti, L. Mesoporous Thin Films: Properties and Applications. *Chem. Soc. Rev.* **2013**, *42*, 4198−4216.
(41) Van Der Voort, P.; Esquivel, D.; De Canck, E.; Goethals, F.; Van Driessche, I.; Romero-Salguero, F. J. Periodic Mesoporous Organosilicas: From Simple to Complex Bridges; a Comprehensive Overview of Functions, Morphologies and Applications. *Chem. Soc. Rev.* **2013**, *42*, 3913−3955.
(42) Park, S. S.; Santha Moorthy, M.; Ha, C. S. Periodic Mesoporous Organosilicas for Advanced Applications. *NPG Asia Mater.* **2014**, *6*, e96.
(43) Volksen, W.; Lionti, K.; Magbitang, T.; Dubois, G. Hybrid Low Dielectric Constant Thin Films for Microelectronics. *Scr. Mater.* **2014**, *74*, 19−24.
(44) Goethals, F.; Ciofi, I.; Madia, O.; Vanstreels, K.; Baklanov, M. R.; Detavernier, C.; Van Der Voort, P.; Van Driessche, I. Ultra-Low-*k* Cyclic Carbon-Bridged PMO Films with a High Chemical Resistance. *J. Mater. Chem.* **2012**, *22*, 8281−8286.
(45) Dubois, G.; Volksen, W.; Magbitang, T.; Miller, R. D.; Gage, D. M.; Dauskardt, R. H. Molecular Network Reinforcement of Sol−Gel Glasses. *Adv. Mater.* **2007**, *19*, 3989−3994.
(46) Dubois, G.; Volksen, W.; Magbitang, T.; Sherwood, M. H.; Miller, R. D.; Gage, D. M.; Dauskardt, R. H. Superior Mechanical Properties of Dense and Porous Organic/Inorganic Hybrid Thin Films. *J. Sol-Gel Sci. Technol.* **2008**, *48*, 187−193.
(47) Bell, R. T.; Jacobs, A. G.; Sorg, V. C.; Jung, B.; Hill, M. O.; Treml, B. E.; Thompson, M. O. Lateral Temperature-Gradient Method for High-Throughput Characterization of Material Processing by Millisecond Laser Annealing. *ACS Comb. Sci.* **2016**, *18*, 548−558.
(48) Jiang, T.; Zhu, B.; Ding, S.; Fan, Z.; Zhang, D. W. High-Performance Ultralow Dielectric Constant Carbon-Bridged Mesoporous Organosilica Films for Advanced Interconnects. *J. Mater. Chem. C* **2014**, *2*, 6502−6510.
(49) Fu, S.; Qian, K.; Ding, S.; Zhang, D. W. Preparation and Characterization of Ultralow-Dielectric Constant Porous SiCOH Thin Films Using 1,2-Bis(triethoxysilyl)ethane, Triethoxymethylsilane, and a Copolymer Template. *J. Electron. Mater.* **2011**, *40*, 2139−2146.
(50) Iyengar, K.; Jung, B.; Willemann, M.; Clancy, P.; Thompson, M. O. Experimental Determination of Thermal Profiles during Laser Spike Annealing with Quantitative Comparison to 3-dimensional Simulations. *Appl. Phys. Lett.* **2012**, *100*, 211915.
(51) Grill, A. Plasma Enhanced Chemical Vapor Deposited SiCOH Dielectrics: From Low-*k* to Extreme Low-*k* Interconnect Materials. *J. Appl. Phys.* **2003**, *93*, 1785−1790.
(52) Launer, P. J. Infrared Analysis of Organosilicon Compounds: Spectra-Structure Correlations. In *Silicon Compounds: Register and Review*; Arkles, B., Ed.; Gelest, Inc.: Morrisville, PA, 2013; pp 175−179.
(53) Lin-Vien, D.; Colthurp, N. B.; Fateley, W. G.; Grasselli, J. G. In *The Handbook of Infrared and Raman Characteristic Frequencies of Organic Molecules*; Academic Press: San Diego, CA, 1991; Chapter 2, pp 9−13.
(54) Zenasni, A.; Jousseaume, V.; Holliger, P.; Favennec, L.; Gourhant, O.; Maury, P.; Gerbaud, G. The Role of Ultraviolet Radiation during Ultralow *k* Films Curing: Strengthening Mechanisms and Sacrificial Porogen Removal. *J. Appl. Phys.* **2007**, *102*, 094107.
(55) Rauda, I. E.; Buonsanti, R.; Saldarriaga-Lopez, L. C.; Benjauthrit, K.; Schelhas, L. T.; Stefik, M.; Augustyn, V.; Ko, J.; Dunn, B.; Wiesner, U.; Milliron, D. J.; Tolbert, S. H. General Method for the Synthesis of Hierarchical Nanocrystal-Based Mesoporous Materials. *ACS Nano* **2012**, *6*, 6386−6399.
(56) Rauda, I. E.; Saldarriaga-Lopez, L. C.; Helms, B. A.; Schelhas, L. T.; Membreno, D.; Milliron, D. J.; Tolbert, S. H. Nanoporous

DOI: 10.1021/acsaelm.9b00205
ACS Appl. Electron. Mater. XXXX, XXX, XXX−XXX

Semiconductors Synthesized Through Polymer Templating of Ligand-Stripped CdSe Nanocrystals. *Adv. Mater.* **2013**, *25*, 1315−1322.
(57) Warren, S. C.; Messina, L. C.; Slaughter, L. S.; Kamperman, M.; Zhou, Q.; Gruner, S. M.; DiSalvo, F. J.; Wiesner, U. Ordered Mesoporous Materials from Metal Nanoparticle−Block Copolymer Self-Assembly. *Science* **2008**, *320*, 1748−1752.

DOI: 10.1021/acsaelm.9b00205
ACS Appl. Electron. Mater. XXXX, XXX, XXX−XXX